Journal of the ICRU Vol 7 No 1 (2007) Report 77
Oxford University Press
doi:10.1093/jicru/ndm013

6 MULTIPLE-SCATTERING ANGULAR DEFLECTIONS

Monte Carlo codes for simulation of high-energy electron and positron transport use 'condensed-history' strategies to describe the global effect of the multiple interactions suffered by an electron or positron along a trajectory segment of a given length s (Berger, 1963). For the simulation of multiple elastic scattering, the basic required information is the angular distribution, relative to the initial direction, of electrons that have traveled the specified path length within the medium. This distribution can be calculated from the theories of Goudsmit and Saunderson (1940) and Lewis (1950).

6.1 GOUDSMIT–SAUNDERSON MULTIPLE-SCATTERING DISTRIBUTION

We consider electrons (or positrons) with kinetic energy E moving in a hypothetical infinite homogeneous medium, with $\mathcal{N}$ scattering centers per unit volume [Eq. (1.7)], in which only elastic collisions occur. We assume that the single-scattering DCS, $\mathrm{d}\sigma(\theta)/\mathrm{d}\Omega$, depends only on the polar scattering angle θ, *i.e.*, it is axially symmetric about the direction of incidence. This assumption is satisfactory as long as the scattering centers are spherically symmetrical atoms or randomly oriented molecules. Moreover, interference effects resulting from coherent scattering by several centers are assumed to be negligible. As a consequence, the theory is applicable only to amorphous materials and to polycrystalline solids. For simplicity, we limit our considerations to single-element materials; the generalization to compounds is straightforward.

The mean free path λ between elastic collisions is given by

$$\lambda = \frac{1}{\mathcal{N}\sigma}, \tag{6.1}$$

where σ is the total cross-section for elastic scattering, Eq. (1.2). The angular distribution $f_1(\theta)$ after a single-scattering event is

$$f_1(\theta) = \frac{1}{\sigma}\frac{\mathrm{d}\sigma(\theta)}{\mathrm{d}\Omega}. \tag{6.2}$$

The probability of elastic scattering for a polar scattering angle between θ and $\theta + \mathrm{d}\theta$ in a single collision is equal to $2\pi f_1(\theta)\sin\theta\,\mathrm{d}\theta$. It is convenient to write $f_1(\theta)$ in the form of a Legendre series

$$f_1(\theta) = \sum_{\ell=0}^{\infty}\frac{2\ell+1}{4\pi}F_\ell\,P_\ell(\cos\theta), \tag{6.3}$$

where P_ℓ are the Legendre polynomials and

$$\begin{aligned} F_\ell &\equiv 2\pi\int_{-1}^{1}P_\ell(\cos\theta)f_1(\theta)\mathrm{d}(\cos\theta) \\ &= \langle P_\ell(\cos\theta)\rangle_1, \end{aligned} \tag{6.4}$$

where the subscript '1' indicates average values for a single collision.

Let us assume that an electron starts off from a certain position, which we select as the origin of our reference frame, moving in the direction of the z axis. An exact Legendre expansion of the multiple-scattering angular distribution was derived by Goudsmit and Saunderson (1940) as follows. Let $F_{\mathrm{GS}}(\theta; s)$ denote the probability distribution function (PDF) of finding the electron moving in the direction (θ, ϕ) after traveling a path length s. Owing to the axial symmetry of the problem, this PDF is independent of the azimuthal angle. Considering the Legendre expansion of the single-scattering distribution given by Eq. (6.3) and using a folding property of the Legendre polynomials, the angular distribution after exactly n collisions is found to be

$$f_n(\theta) = \sum_{\ell=0}^{\infty}\frac{2\ell+1}{4\pi}(F_\ell)^n P_\ell(\cos\theta). \tag{6.5}$$

We recall that the inverse mean free path λ^{-1} gives the collision probability per unit path length. This result implies that the probability distribution for a number n of collisions after a path length s is Poissonian with mean $\langle n\rangle = s/\lambda$, *i.e.*,

$$P(n) = \exp(-s/\lambda)\frac{(s/\lambda)^n}{n!}. \tag{6.6}$$

The angular distribution after a path length s can then be expressed as

$$F_{\rm GS}(\theta;s) = \sum_{n=0}^{\infty} P(n) f_n(\theta) = \sum_{\ell=0}^{\infty} \frac{2\ell+1}{4\pi} \times \left[\exp(-s/\lambda) \sum_{n=0}^{\infty} \frac{(s/\lambda)^n}{n!} (F_\ell)^n \right] P_\ell(\cos\theta).$$

Introducing the coefficients

$$G_\ell \equiv \frac{1-F_\ell}{\lambda} = \mathcal{N}\sigma 2\pi \int_{-1}^{1} [1 - P_\ell(\cos\theta)] f_1(\theta)\, \mathrm{d}(\cos\theta), \qquad (6.7)$$

the multiple-scattering distribution can be finally written in the form

$$F_{\rm GS}(\theta;s) = \sum_{\ell=0}^{\infty} \frac{2\ell+1}{4\pi} \exp(-sG_\ell) P_\ell(\cos\theta), \qquad (6.8)$$

which is the expansion derived by Goudsmit and Saunderson. Notice that $F_0 = 1$ and $G_0 = 0$. The value of F_ℓ decreases with ℓ owing to the increasingly faster oscillations of $P_\ell(\cos\theta)$ and, hence, G_ℓ increases monotonically with ℓ and tends to λ^{-1} when ℓ goes to infinity. Figure 6.1a shows Goudsmit–Saunderson distributions of 10 MeV electrons in gold for different path lengths s, given as multiples of the mean free path λ. In these calculations we used the DCS from the present database (obtained from Dirac partial-wave analysis with the F–DF–FM potential); the corresponding mean free path is 4.25×10^{-5} g/cm^2. As these multiple-scattering angular distributions have been calculated neglecting energy loss, they are realistic only for relatively short path lengths, such that the average fractional energy loss is small. We see that the angular distribution widens progressively when the number of collisions $\langle n\rangle = s/\lambda$ increases. Figure 6.1b displays the coefficients $(2\ell+1)\exp(-sG_\ell)$ of the Legendre series for the same path lengths (notice that for $\ell = 0$, the coefficient is equal to unity). It is clear that the convergence the series improves rapidly when s increases. In the limit $s \to \infty$, only the term $\ell = 0$ contributes and the distribution becomes isotropic, $F_{\rm FS}(\theta; s) \to (4\pi)^{-1}$.

The ℓth transport mean free path, λ_ℓ, is defined by [Eq. (1.6)]

$$\lambda_\ell = G_\ell^{-1} = (\mathcal{N}\sigma_\ell)^{-1}, \qquad (6.9)$$

where σ_ℓ is the ℓth transport cross-section, Eq. (1.3). The first inverse transport mean free path,

$$\lambda_1^{-1} = G_1 = \frac{2\pi}{\lambda} \int_{-1}^{1} [1 - \cos\theta]\, f_1(\theta)\, \mathrm{d}(\cos\theta) = \frac{\langle 1 - \cos\theta\rangle_1}{\lambda}, \qquad (6.10)$$

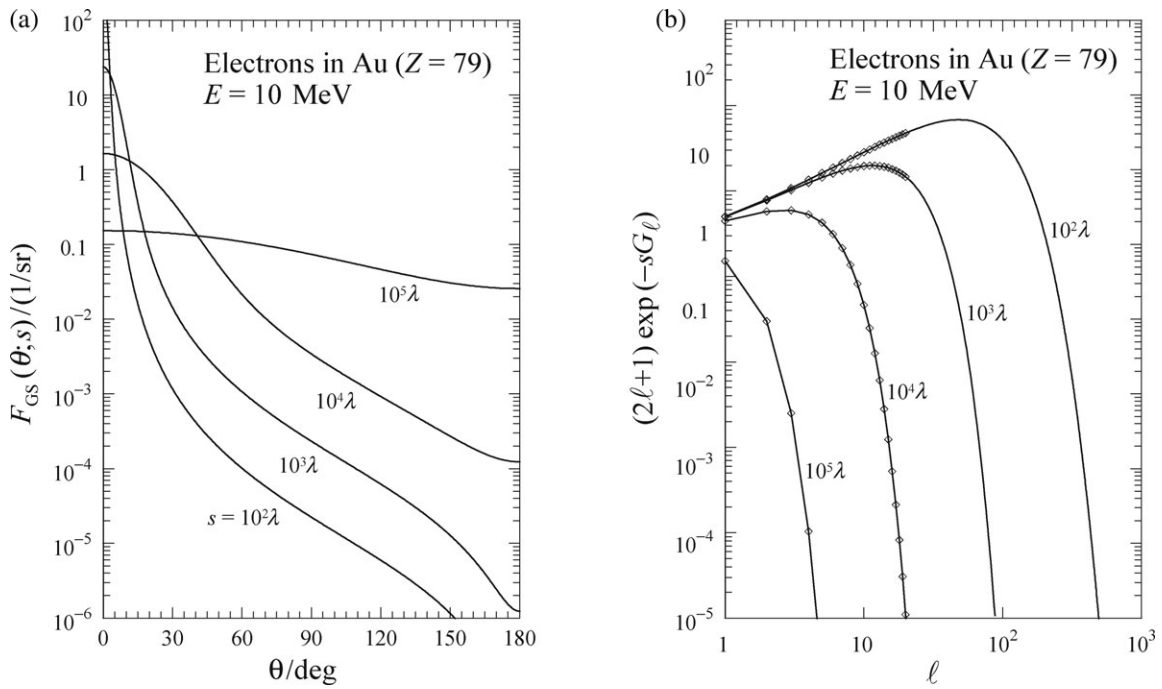

Figure 6.1. (a) Goudsmit–Saunderson angular distributions, Eq. (6.8), of 10 MeV electrons in gold for various path lengths s, given in units of the mean free path λ. (b) Coefficients $(2\ell+1)\exp(-sG_\ell)$ of the Legendre series, Eq. (6.8), for the same path lengths.

gives a measure of the average angular deflection per unit path length. By analogy with the 'stopping power', which is defined as the mean energy loss per unit path length (see below), λ_1^{-1} is sometimes called the 'scattering power'.

From the orthogonality of the Legendre polynomials, it follows that

$$\langle P_\ell(\cos\theta)\rangle_{\rm GS} \equiv 2\pi\int_{-1}^{1} P_\ell(\cos\theta)F_{\rm GS}(\theta;s)\,{\rm d}(\cos\theta) = \exp(-sG_\ell). \tag{6.11}$$

For $\ell = 0$, this formula gives

$$2\pi\int_{-1}^{1} F_{\rm GS}(\theta;s)\,{\rm d}(\cos\theta) = 1, \tag{6.12}$$

i.e., the PDF is normalized to unity. For ℓ =1 and 2, Eq. (6.11) implies that

$$\langle\cos\theta\rangle_{\rm GS} = \exp(-sG_1) \tag{6.13}$$

and

$$\langle\cos^2\theta\rangle_{\rm GS} = \frac{1}{3}[1+2\exp(-sG_2)], \tag{6.14}$$

respectively.

The Goudsmit–Saunderson expansion (6.8) and the results (6.13) and (6.14) are exact. To compute these quantities for a given single-scattering DCS, which usually is available only in numerical form, we have to evaluate the transport coefficients G_ℓ as defined in Eq. (6.7). The number of terms needed to get convergence of the Goudsmit–Saunderson series increases as the path length decreases. In the case of small path lengths, the convergence of the series can be improved by separating the contributions from electrons that have had no collisions (Berger and Wang, 1988),

$$F_{\rm GS}(\theta;s) \equiv \exp(-s/\lambda)\frac{\delta(\cos\theta-1)}{\pi} + \sum_{\ell=0}^{\infty}\frac{2\ell+1}{4\pi} \times\left[\exp(-sG_\ell) - \exp\left(\frac{-s}{\lambda}\right)\right]P_\ell(\cos\theta). \tag{6.15}$$

The first term on the right-hand side represents unscattered electrons.

6.1.1 The Wentzel DCS model

In general, the transport coefficients G_ℓ, Eq. (6.7.) must be calculated numerically, and because of the fast oscillations of Legendre polynomials of large orders, the calculation is far from trivial. We shall consider here a simple analytical DCS model that yields an analytical expression for the transport coefficients that, therefore, can be used to check the accuracy of the numerical algorithm used for calculation of the G_ℓ coefficients for arbitrary DCSs. Let us assume that the DCS is approximated as

$$\frac{{\rm d}\sigma^{\rm (W)}(\theta)}{{\rm d}\Omega} = \sigma^{\rm (W)}\frac{A(1+A)}{\pi(2A+1-\cos\theta)^2}. \tag{6.16}$$

This expression has the same angular dependence as the Wentzel DCS, Eq. (C.35), which is the nonrelativistic DCS for the Wentzel potential, Eq. (C.1), obtained within the first Born approximation. Here, however, $\sigma^{\rm (W)}$ and A are considered as adjustable parameters that may be determined, *e.g.*, by fitting a realistic DCS obtained from partial-wave calculations. The factor

$$f_1^{\rm (W)}(\theta) = \frac{A(1+A)}{\pi(2A+1-\cos\theta)^2} \tag{6.17}$$

is the normalized angular PDF for single scattering and, therefore, the total cross-section is equal to $\sigma^{\rm (W)}$. The transport coefficients for the Wentzel DCS, Eq. (6.16.), are (Fernández-Varea *et al.*, 1993)

$$G_\ell^{\rm (W)} = \mathcal{N}\sigma^{\rm (W)}\{1-\ell[Q_{\ell-1}(1+2A) - (1+2A)Q_\ell(1+2A)]\}, \tag{6.18}$$

where $Q_\ell(x)$ are Legendre functions of the second kind (Abramowitz and Stegun, 1974). These functions can be calculated easily from their recurrence relations. The first transport coefficient is

$$G_1^{\rm (W)} = \mathcal{N}\sigma^{\rm (W)}\,2A\left[(1+A)\ln\left(\frac{1+A}{A}\right)-1\right]. \tag{6.19}$$

Given a realistic DCS, with total cross-section σ and first transport cross-section σ_1, we can set $\sigma^{\rm (W)} = \sigma$ and determine the 'screening' parameter A by requiring that $G_1^{\rm (W)} = \mathcal{N}\sigma_1$. The Wentzel DCS, Eq. (6.16), then describes an elastic-scattering process that has the same mean free path and the same single-scattering average deflection as the real process. Because the shape of the Wentzel DCS is physically plausible, it yields multiple-scattering distributions that resemble those of the realistic DCS. The resemblance improves when the path length increases. For relatively large path

lengths, when the average number of interactions is larger than about 20 (the multiple-scattering regime), repeated scattering smears out the details of the DCS and the angular distributions obtained from the realistic DCS and the Wentzel DCS are practically the same.

Molière (1948) (see also Bethe, 1953) derived an approximate analytical expression for the multiple-scattering angular distribution that was used in several popular Monte Carlo codes (Jenkins *et al.*, 1988). Because the Molière distribution is evaluated rapidly for arbitrary path lengths (larger than $\approx 4\lambda$) and can be easily sampled, it is convenient for mixed (class II) simulations (Berger, 1963) in which the step length s fluctuates randomly. Fernández-Varea *et al.* (1993) showed that the Molière theory is essentially equivalent to the Goudsmit–Saunderson theory for a Wentzel model with specific values of the total cross-section $\sigma^{(\mathrm{W})}$ and the parameter A. The DCS underlying Molière's theory is the Wentzel DCS, Eq. (6.16), with the following energy- and Z-dependent screening parameter,

$$A^{(\mathrm{M})} = \frac{1}{4}\frac{(\hbar c)^2}{E(E+2m_\mathrm{e}c^2)}\frac{1.13+3.76Z^2/(137\,\beta)^2}{(0.885Z^{-1/3}a_0)^2}, \tag{6.20}$$

and total elastic-scattering cross-section,

$$\sigma^{(\mathrm{M})} = \frac{(Ze^2)^2}{\beta^2\,E(E+2m_\mathrm{e}c^2)}\frac{\pi}{A^{(\mathrm{M})}(1+A^{(\mathrm{M})})}. \tag{6.21}$$

These expressions were determined by Molière by fitting the elastic DCS obtained from the eikonal approximation with the Thomas–Fermi atomic field. In the following, the Wentzel DCS with Molière's parameters will be referred to as the Wentzel–Molière DCS.

6.2 MULTIPLE SCATTERING DISTRIBUTIONS WITH ENERGY LOSS

A more elaborate theory of multiple elastic scattering, which considers angular deflections and spatial displacements, was formulated by Lewis (1950). This theory accounts also for the effect of energy loss on the multiple-scattering process by means of the CSDA. In this approximation, the projectile is assumed to lose energy continuously along its path and the slowing-down process is completely characterized by the (linear) stopping power $S(E)$, which as mentioned above, is defined as the average energy loss per unit path length,

$$S(E) = -\frac{\mathrm{d}E}{\mathrm{d}s}. \tag{6.22}$$

Tables of stopping powers for multiple materials, including elements and compounds, are given in the ICRU 37 report (ICRU, 1984) for $E \geq 10$ keV. It is worth mentioning that the CSDA completely neglects energy straggling, *i.e.*, fluctuations in the energy loss due to the discreteness of the energy transfers in inelastic and radiative interactions and to the randomness of the number of these interactions. A consistent multiple-scattering theory, including an accurate treatment of energy straggling, could be formulated only in numerical form and would be too complicated to be useful in general-purpose Monte Carlo simulation codes.

The CSDA sets a strict correspondence between path length and energy loss. The CSDA range of an electron with kinetic energy E is given by

$$R(E) = \int_{E_\mathrm{abs}}^{E} \frac{\mathrm{d}E'}{S(E')}, \tag{6.23}$$

where E_abs is the 'absorption' energy, *i.e.*, the energy at which the electron is assumed to be effectively absorbed in the medium. If an electron starts its trajectory with kinetic energy E, the energy loss W after a path length s is determined by the equation

$$s = \int_{E-W}^{E} \frac{\mathrm{d}E'}{S(E')} = R(E) - R(E-W). \tag{6.24}$$

Hence, to calculate the energy loss as a function of the path length, $W(s)$, we only need to know the CSDA range as a function of energy, $R(E)$. The average number of elastic collisions undergone by the electron along the path length s is

$$\langle n \rangle = \int_0^s \frac{\mathrm{d}s'}{\lambda(s')} = \int_{E-W(s)}^{E} \frac{1}{\lambda(E')}\frac{\mathrm{d}E'}{S(E')}. \tag{6.25}$$

Notice that λ here is first regarded as a function of the path length s and, afterward, as a function of the 'local' energy $E' = E - W(s)$.

Let us consider an electron that starts from the origin of our reference frame and moves in the direction of the z-axis. Let $f(\boldsymbol{r}, \hat{\boldsymbol{d}}; s)$ denote the probability density of finding the electron at the position $\boldsymbol{r} = (x, y, z)$, moving in the direction given by the unit vector $\hat{\boldsymbol{d}}$ after having traveled a path length s. The diffusion equation for this problem is

(Lewis, 1950)

$$\frac{\partial f}{\partial s}+\hat{\boldsymbol{d}}\cdot\nabla f=\mathcal{N}\int\Big[f(\boldsymbol{r},\hat{\boldsymbol{d}}';s)-f(\boldsymbol{r},\hat{\boldsymbol{d}};s)\Big]\times\frac{\mathrm{d}\sigma(\chi;s)}{\mathrm{d}\Omega}\,\mathrm{d}\Omega, \tag{6.26}$$

where $\chi\equiv\cos^{-1}(\hat{\boldsymbol{d}}\cdot\hat{\boldsymbol{d}}')$ is the scattering angle corresponding to the angular deflection $\hat{\boldsymbol{d}}'\rightarrow\hat{\boldsymbol{d}}$ and $\mathrm{d}\sigma(\chi;s)/\mathrm{d}\Omega$ is the elastic DCS for an electron with the energy $E-W(s)$. This equation has to be solved under the boundary condition $f(\boldsymbol{r},\hat{\boldsymbol{d}};0)=(1/\pi)\delta(\boldsymbol{r})\,\delta(1-\cos\theta)$, where θ is the polar angle of the direction $\hat{\boldsymbol{d}}$. By expanding $f(\boldsymbol{r},\hat{\boldsymbol{d}};s)$ in spherical harmonics, Lewis (1950) obtained general expressions for the angular distribution and for the first moments of the spatial distribution after a given path length s. The angular distribution is given by

$$F_{\mathrm{L}}(\theta;s)\equiv\int f(\boldsymbol{r},\hat{\boldsymbol{d}};s)\,\mathrm{d}\boldsymbol{r}=\sum_{\ell=0}^{\infty}\frac{2\ell+1}{4\pi}\exp[-\mathcal{G}_\ell(s)]P_\ell(\cos\theta), \tag{6.27}$$

where

$$\mathcal{G}_\ell(s)=\int_0^s G_\ell(s')\mathrm{d}s'=\int_{E-W(s)}^{E}\frac{G_\ell(E')}{\rho}\frac{\mathrm{d}E'}{S(E')/\rho}. \tag{6.28}$$

In the last expression, G_ℓ and S are considered as functions of kinetic energy of the projectile. $(G_\ell/\rho)^{-1}=\rho\lambda_\ell$ is the ℓth transport mean free path, see Eq. (6.9), in mass-thickness units (g/cm^2) and $S(E)/\rho$ is the mass stopping power (in eV cm^2/g). The result from Eq. (6.27) reduces to the distribution of Goudsmit and Saunderson, Eq. (6.8), when the energy loss is negligible.

For small path lengths, the Legendre expansion (6.27) converges very slowly, mainly due to the contribution of unscattered electrons which is proportional to $\delta(\cos\theta-1)$. It is then advantageous to separate the contribution from electrons that have undergone no collisions,

$$F_{\mathrm{L}}(\theta;s)\equiv\exp(-\langle n\rangle)\frac{\delta(\cos\theta-1)}{\pi}+\sum_{\ell=0}^{\infty}\frac{2\ell+1}{4\pi}[\exp(-\mathcal{G}_\ell)-\exp(-\langle n\rangle)]P_\ell(\cos\theta). \tag{6.29}$$

The average values of the Legendre polynomials take simple expressions,

$$\langle P_\ell(\cos\theta)\rangle_{\mathrm{L}}\equiv 2\pi\int_{-1}^{1}P_\ell(\cos\theta)F_{\mathrm{L}}(\theta;s)\;\mathrm{d}(\cos\theta)=\exp[-\mathcal{G}_\ell(s)]. \tag{6.30}$$

In particular,

$$\langle\cos\theta\rangle_{\mathrm{L}}=\exp[-\mathcal{G}_1(s)], \tag{6.31}$$

and

$$\langle\cos^2\theta\rangle_{\mathrm{L}}=\frac{1}{3}\{1+2\exp[-\mathcal{G}_2(s)]\}. \tag{6.32}$$

Lewis (1950) also derived closed formulas for the first moments of the spatial distribution, $\langle z\rangle_{\mathrm{L}}$ and $\langle x^2+y^2\rangle_{\mathrm{L}}$, and for the correlation function of z and $\cos\theta$, $\langle z\cos\theta\rangle_{\mathrm{L}}$.

Negreanu *et al.* (2005) have described an efficient method for the calculation of the Goudsmit–Saunderson multiple-scattering coefficients G_ℓ. Their algorithm takes advantage of peculiarities of the Gauss–Legendre quadrature formula to compute a large number of coefficients (up to 15,000) simultaneously. The computer codes GOUDSMIT and LEWIS, included in the CD-ROM that accompanies the present report, use this numerical algorithm to calculate accurate multiple-scattering distributions for pure elements and a large number of compounds using the theories of Goudsmit and Saunderson and of Lewis, respectively. These programs read auxiliary numerical files, specific for each material, that contain composition data, inelastic-scattering parameters and tables of stopping powers for electrons and positrons. These auxiliary files were generated by using the preprocessing program MATERIAL of the Monte Carlo code system PENELOPE (Salvat *et al.*, 2003). The stopping powers calculated by MATERIAL are essentially equivalent to those recommended in the ICRU 37 report (ICRU, 1984), but extend to lower energies.

Figure 6.2 displays multiple-scattering angular distributions of 15.7 MeV electrons in gold that were measured by Hanson *et al.* (1951). In their experiment, an electron beam with an angular width of about 1° was focused on a thin scattering foil of gold; the converging beam had a full angular width of about 1°. The angular distribution of electrons transmitted through the foil was measured by collecting all electrons with energy within 6 % of the maximum energy emerging in various directions. The theoretical distributions shown in

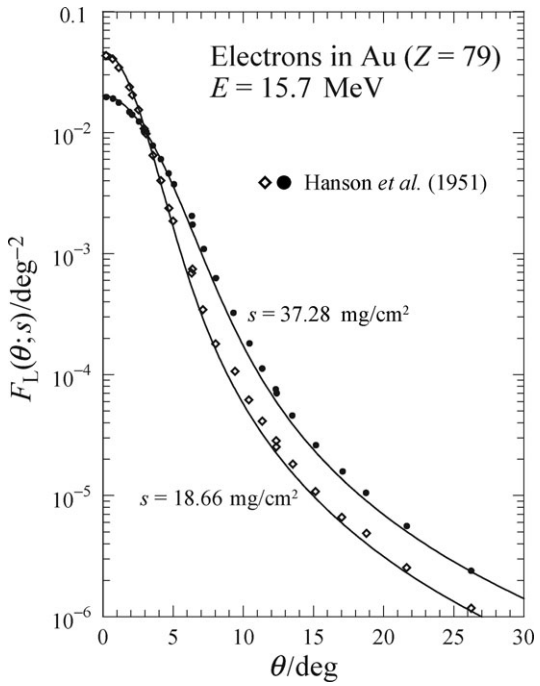

Figure 6.2. Angular distribution of 15.7 Mev electrons transmitted thorough gold scattering foils of the indicated thicknesses. Symbols are experimental data from Hanson *et al.* (1951), and the curves represent the angular distribution calculated from the Lewis theory, Eq. (6.29), with s equal to the foil thickness. From Negreanu *et al.* (2005).

Figure 6.2. were calculated using the program LEWIS, *i.e.*, from the Lewis formula, Eq. (6.29), with the partial-wave DCSs from the present database and the stopping powers calculated by the program MATERIAL. The path length s was set equal to the thickness of the scattering foil. For the thicker foil (37.28 mg/cm^2), the CSDA energy loss is 0.75 % of the initial energy and $\langle \cos\,\theta \rangle_{\,\mathrm{L}} = 0.995$. Therefore, the slight differences between the theory and the experiment are very likely due to the finite angular extent of the incident beam.

6.3 CONTRIBUTION OF INELASTIC COLLISIONS

For practical Monte Carlo simulations of high-energy electron/positron transport (Jenkins *et al.*, 1988), it is of interest to consider the angular deflections of the projectile due to inelastic collisions. Several popular Monte Carlo codes describe the energy loss resulting from multiple inelastic collisions by means of the theory of Landau (1944) or one of its various improved versions. These energy-straggling theories do not account for deflection in inelastic scattering, and other means have to be utilized to overcome this deficiency. The inelastic-scattering DCS, differential in scattering angle, can be calculated approximately from the Morse formula [Inokuti (1971), Eq. (4.70)], which expresses the angular DCS in terms of the incoherent scattering function. This approach was followed by Fano (1954) in order to introduce electron-scattering effects into the multiple-scattering theory of Molière (1948). However, the DCS calculated in this way is only a rough approximation and, moreover, it accounts for all excitations.

A more consistent method to calculate the inelastic-scattering angular DCS is to consider the first Born approximation (Fano, 1963; Inokuti, 1971) with an empirical model of the generalized oscillator strength. The angular DCSs can then be obtained by integrating the Born DCS (differential in energy loss and scattering angle) over energy loss. The practical approach is to use semi-empirical optical-data models of the inelastic-scattering DCS, which are built by combining optical properties of the medium (experimental refractive index and extinction coefficient data, and theoretical photoabsorption cross-sections if needed) with suitable extension algorithms, usually based on the free-electron gas theory. A relativistic optical-data model, which is tailored for Monte Carlo simulation of electron and positron transport, has been described by Fernández-Varea *et al.* (2005). Although approximate, this model provides fairly accurate estimates of quantities that result from integration over kinematically allowed energy losses, an example of which is the angular DCS.

Figures 6.3 and 6.4 display elastic DCSs, $\mathrm{d}\sigma/\mathrm{d}\Omega$, and inelastic angular DCSs, $\mathrm{d}\sigma_{\mathrm{in}}/\mathrm{d}\Omega$, for collisions of electrons of different energies with water and gold. The inelastic DCSs were calculated by using the optical-data model of Fernández-Varea *et al.* (2005) with the experimental optical oscillator strengths of liquid water (Dingfelder *et al.*, 1998) and solid gold, *i.e.*, these inelastic DCSs pertain to the condensed phase. The sudden drop of the inelastic DCS is due to the indistinguishability of the projectile and the electron ejected in a hard inelastic collision; the primary electron is considered as the faster of the two, and this convention forbids scattering angles larger than a certain cutoff angle θ_{c} which varies with the energy of the projectile. Positron-inelastic DCSs have a shape similar to those for electrons of the same energy at small angles, but decrease monotonically beyond the electron cutoff angle and fall to zero at 90°. Scattering angles larger than 90° are kinematically forbidden (*i.e.*, in a binary collision of two particles of equal mass, backscattering of the projectile would violate conservation of either energy or momentum).

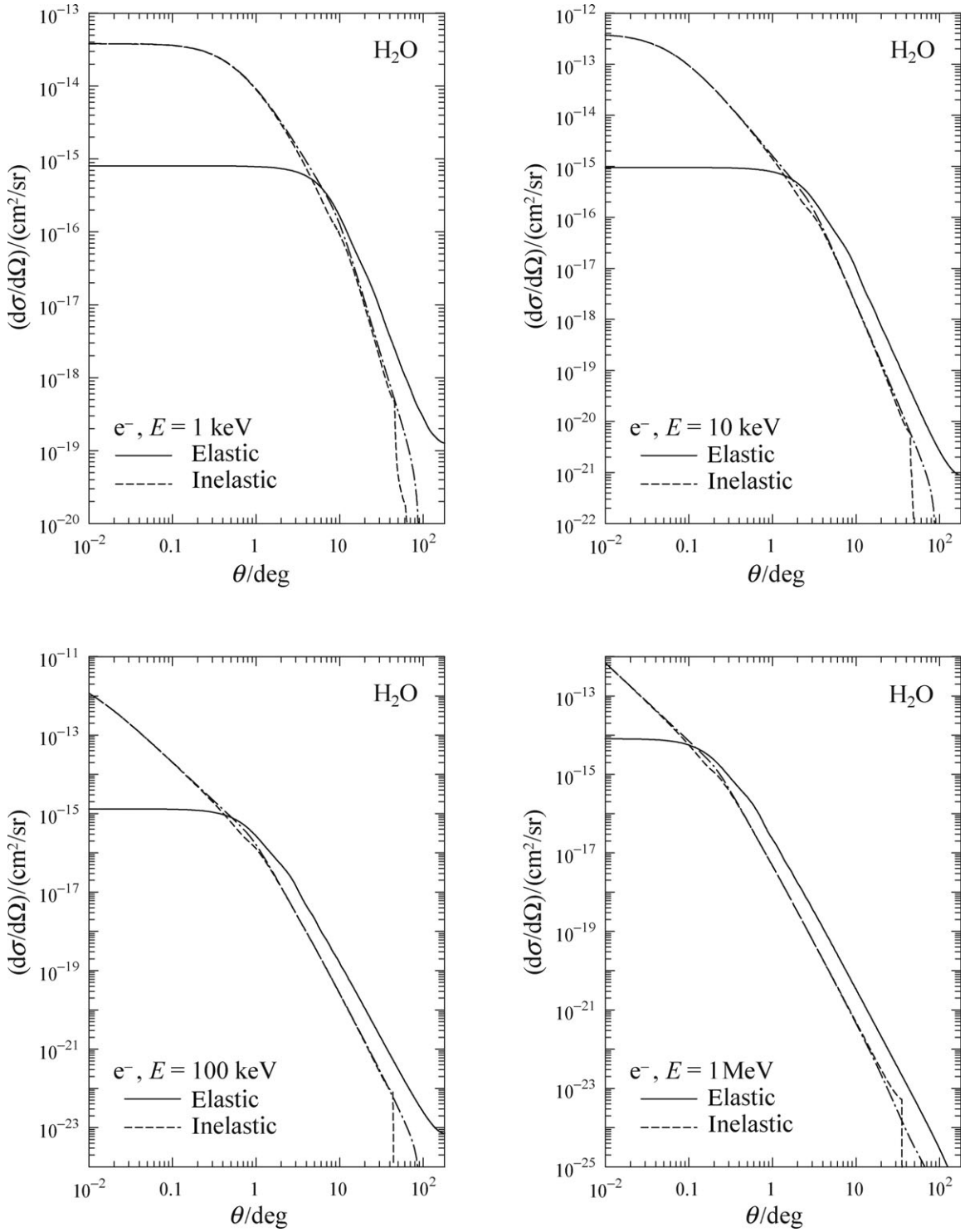

Figure 6.3. DCSs for elastic and inelastic scattering of electrons in water. Elastic cross-sections (solid lines) were calculated using the independent-atom approximation, Eq. (3.80), with the F-DF potential for the atoms. The dashed lines represent DCSs for inelastic scattering of electrons calculated from the optical-data model of Fernández-Varea *et al.* (2005) with the empirical optical oscillator strength of liquid water (Dingfelder *et al.*, 1998). The dash-dotted lines are angular DCSs for inelastic scattering of positrons.

Elastic and inelastic angular distributions have manifestly different shapes. The inelastic DCS is more strongly peaked at small angles where it exceeds the elastic DCSs by several orders of magnitude. However, for projectiles with sufficiently large kinetic energies (depending on the atomic number of the target), the inelastic angular DCS is approximately equal to Z^{-1}

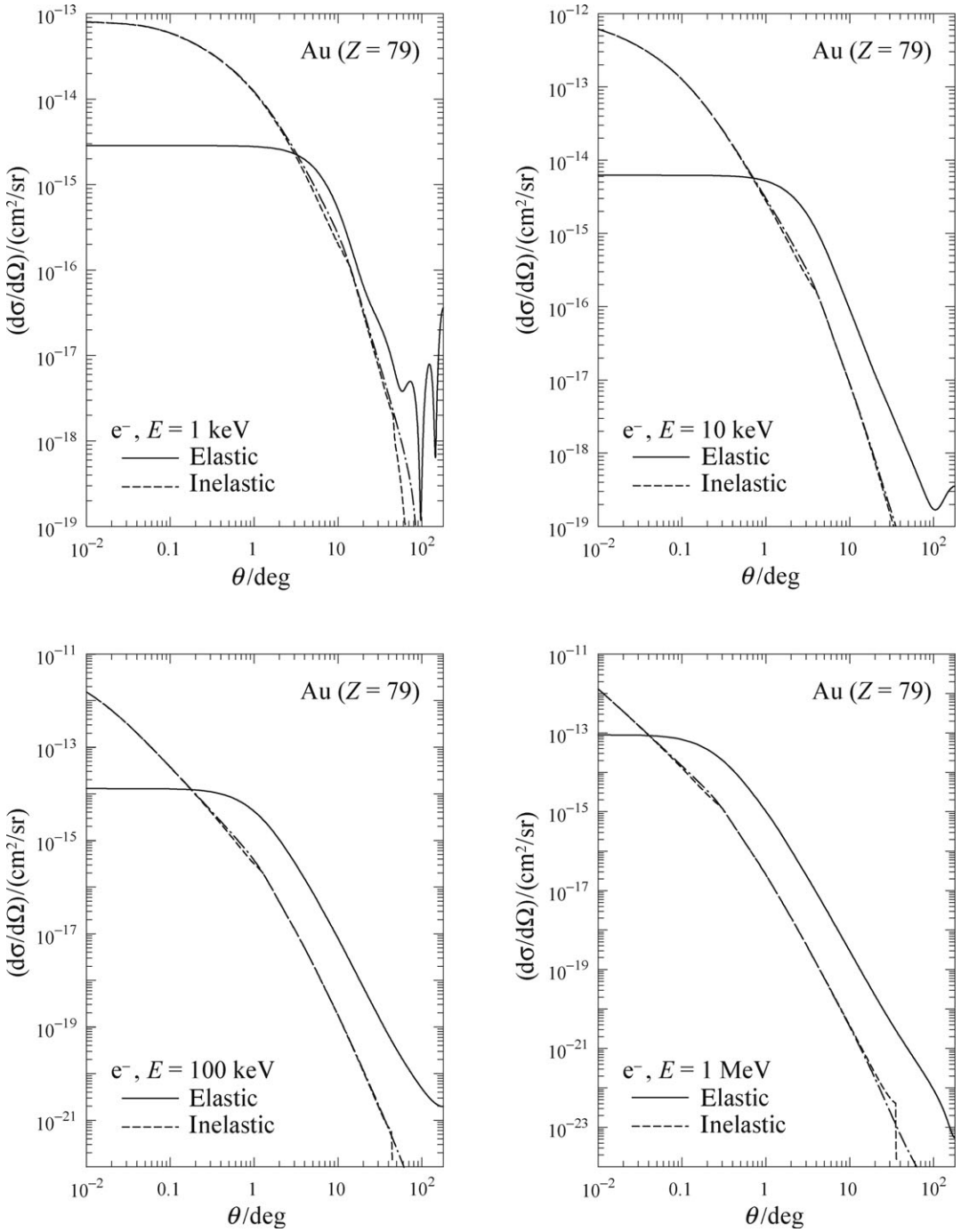

Figure 6.4. DCSs for elastic and inelastic scattering of electrons in gold. Elastic cross-sections (solid lines) were calculated using the static-exchange approximation with the F-DF potential for free atoms. The dashed lines represent DCSs for inelastic scattering of electrons calculated from the optical-data model of Fernández-Varea *et al.* (2005) with the empirical optical oscillator strength of solid gold. The dash-dotted lines are angular DCSs for inelastic scattering of positrons.

times the elastic DCS for a relatively wide interval of scattering angles. This similarity, which holds for all elements, justifies a commonly used approximation in which the effect of inelastic collisions is introduced by multiplying the elastic DCS by $1 + Z^{-1}$. This approximation fails only for small scattering angles (which are of no practical importance for multiple-scattering processes) and above the kinematical cutoff. As noted by Seltzer (1988), the latter limitation can be corrected by simply multiplying the multiple-scattering distribution by the factor $Z/(1 + Z)$ at all angles greater than the kinematical cutoff angle θ_c.

Total and transport cross-sections for elastic and inelastic scattering of electrons by water and gold are displayed in Fig. 6.5. Inelastic transport cross-sections are always smaller than those for elastic scattering. For electrons and positrons with energies larger than about 10 keV, the relative importance of inelastic scattering decreases when the atomic number of the material increases.

To account for the effect of inelastic scattering within the multiple-scattering theories of Goudsmit and Saunderson and of Lewis, the transport coefficients G_ℓ, Eq. (6.7), must be calculated for the sum of the elastic DCS and the inelastic angular DCS,

$$G_\ell = \mathcal{N}\, 2\pi \int_{-1}^{1} [1 - P_\ell(\cos\theta)] \times \left[\frac{\mathrm{d}\sigma(\theta)}{\mathrm{d}\Omega} + \frac{\mathrm{d}\sigma_{\mathrm{in}}(\theta)}{\mathrm{d}\Omega}\right] \mathrm{d}(\cos\theta), \qquad (6.33)$$

where $\mathrm{d}\sigma_{\mathrm{in}}/\mathrm{d}\Omega$ is the inelastic angular DCS.

Various Monte Carlo codes for high-energy electron and positron transport use mixed simulation schemes (Berger, 1963; Salvat *et al.*, 2003) in which hard inelastic collisions, with energy loss larger than a given cutoff value W_c, are simulated individually. In these mixed simulations, the adopted multiple-scattering angular distribution should account only for the deflections caused by the soft inelastic collisions, *i.e.*, those with energy losses less than the cutoff energy W_c. That is, the inelastic angular DCS in Eq. (6.33) must be restricted to energy losses less than W_c.

The programs GOUDSMIT and LEWIS implement the following simple analytical models of the inelastic angular DCS (Negreanu *et al.*, 2005).

(1) The inelastic DCS is set equal to Z^{-1} times the elastic DCS. As mentioned above, this approximation is valid only for relatively fast projectiles and intermediate scattering angles. It is useful to estimate the magnitude of inelastic corrections in terms of only the elastic DCS.
(2) The inelastic DCS is obtained from the Morse formula using the parameterization of the incoherent-scattering function given by Baró *et al.* (1994).
(3) The inelastic angular DCS is calculated from the first Born approximation with the Sternheimer–Liljequist generalized oscillator strength model (see Salvat *et al.*, 2003, and references therein). This model provides a simple, but fairly realistic, description of inelastic collisions.

    It is used in the Monte Carlo program PENELOPE (Salvat *et al.*, 2003) to simulate inelastic collisions and has also been utilized to compute the collision stopping powers used in the program LEWIS.

Negreanu *et al.* (2005) have shown that the Morse formula and the Sternheimer–Liljequist

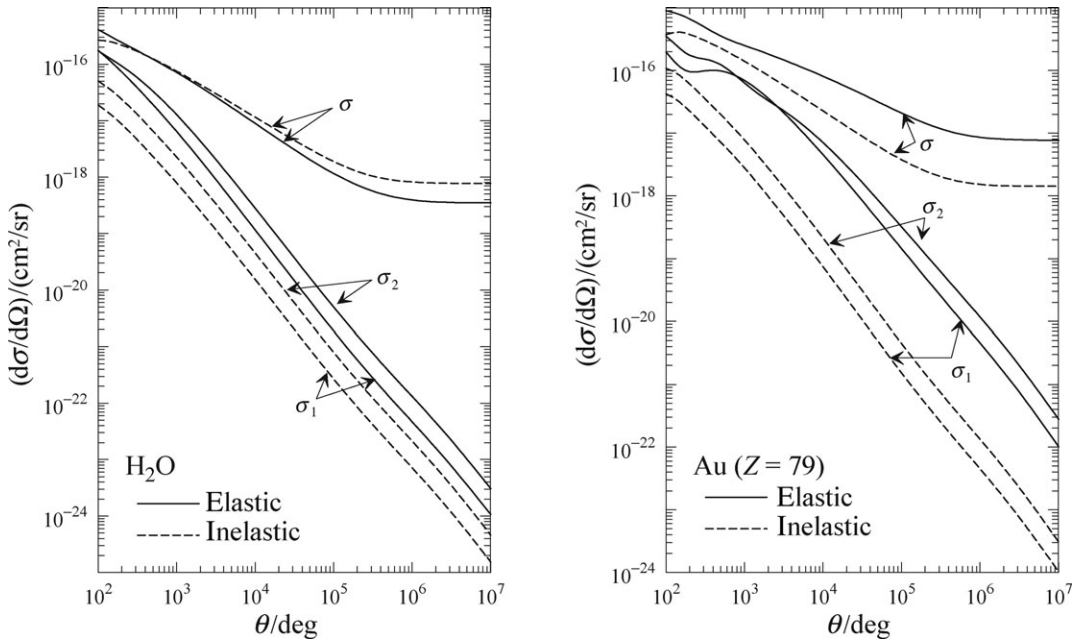

Figure 6.5. Total cross-sections and first and second transport cross-sections for elastic and inelastic scattering of electrons by water and gold. Elastic cross-sections were calculated using the F-DF-FM potential. The inelastic DCS was calculated from the optical data model with the empirical optical oscillator strengths of liquid water and metallic gold.

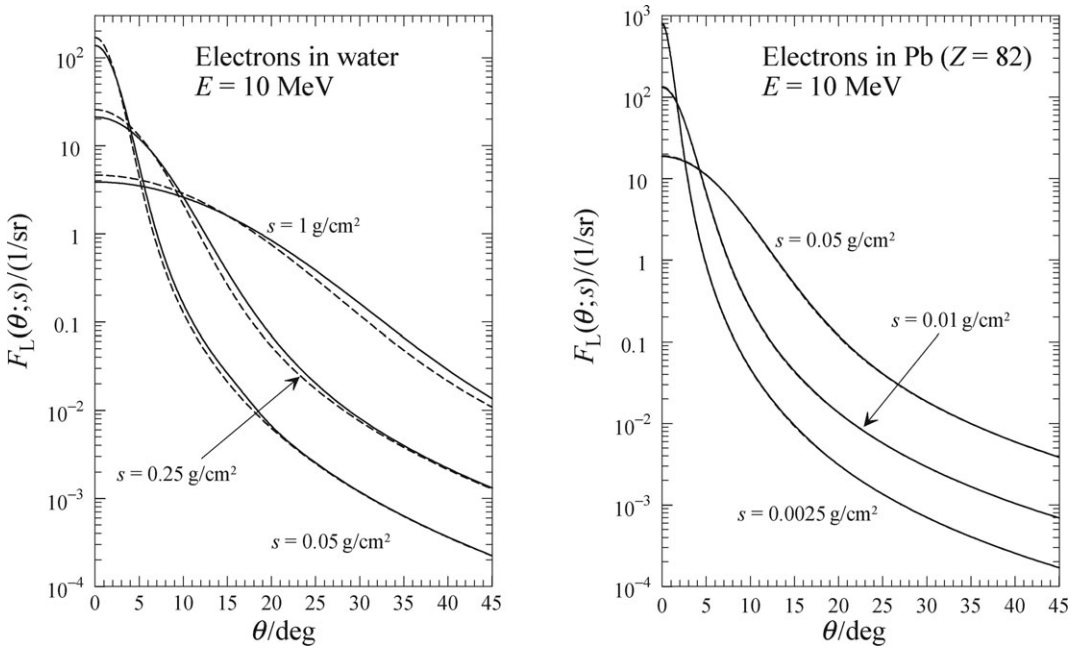

Figure 6.6. Lewis multiple-scattering angular distributions of 10 MeV electrons after traveling the indicated path lengths in water and lead. The solid curves were generated by the program LEWIS using elastic DCSs from the present database and inelastic DCSs obtained from the Sternheimer–Liljequist model. The dashed curves are results from similar calculations without the inelastic contribution.

model yield similar inelastic-scattering DCSs, except at very small scattering angles, where the latter model is deemed to be more reliable. Inclusion of inelastic scattering with these two models slows down the convergence of the Legendre expansion of the multiple scattering distribution, because the inelastic angular DCS peaks sharply at small angles and vanishes for $\theta \geq 90^\circ$.

Figure 6.6 shows multiple-scattering angular distributions of 10 MeV electrons in water and lead that were calculated by the program LEWIS using elastic DCSs from the present database. Inelastic DCSs were obtained from the Sternheimer–Liljequist DCS model, and stopping powers were generated by the pre-processing program MATERIAL of the PENELOPE code system. To show the effect of inelastic scattering, multiple-scattering distributions calculated by considering only elastic deflections are also displayed. In these examples, inelastic scattering is significant only for water.

6.4 INFLUENCE OF ELASTIC-SCATTERING DATA ON MULTIPLE-SCATTERING CALCULATIONS

The angular distributions from multiple-scattering calculations can depend on the adopted elastic DCS model. For path lengths of the order of a few times the elastic mean free path, the average number of collisions is small (plural scattering) and the multiple-scattering distributions depend strongly on the adopted DCS. When the path length increases, the angular distribution becomes broader and the details of the multiple-scattering distribution are progressively washed out. When the path length approaches the CSDA range, the angular distribution becomes isotropic and, therefore, independent of the adopted DCS.

To illustrate the sensitivity of multiple-scattering angular distributions to the adopted DCS, we consider the case of 20 MeV electrons in water and lead. Figure 6.7 compares angular distributions for different path lengths in these two materials calculated by the program LEWIS using the partial-wave DCSs from the present database and the Wentzel–Molière DCS model [Eqs. (6.16) and (6.20–21)]. It is worth noting that the slowing down of the projectile was accounted for within the CSDA in these calculations. Therefore, the distributions calculated with the Wentzel–Molière DCS model are not comparable to those given by the original theory of Molière (1948) which disregards the slowing down of the electron along its trajectory. In the case of water, the Wentzel–Molière DCS yields results in close agreement with those obtained from the partial-wave DCS, in spite of the approximate nature of the DCS given by Eq. (6.16). This agreement explains why Monte Carlo codes based on the Molière theory provide reliable results for electron transport in water and biological materials. For other materials, however, the distributions

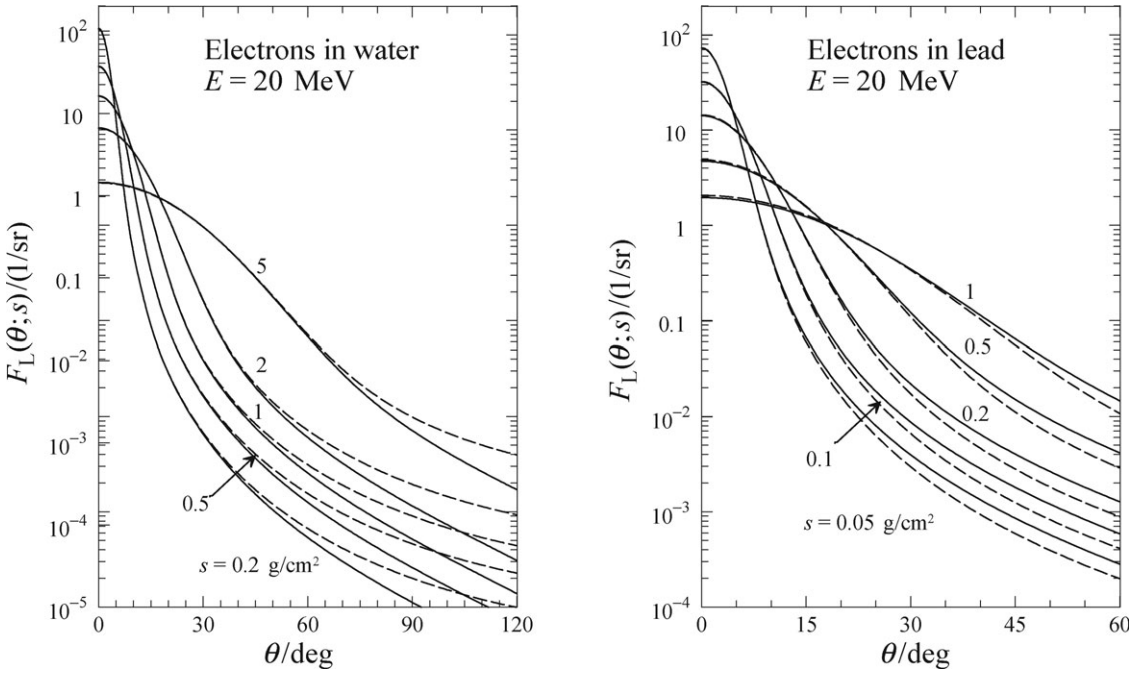

Figure 6.7. Multiple-scattering angular distributions of 20 MeV electrons after traveling the indicated path lengths in water and lead that were generated by the program LEWIS. The continuous curves represent distributions calculated using elastic partial-wave DCSs from the present database. The dashed curves are results from similar calculations using the Wentzel–Molière DCS.

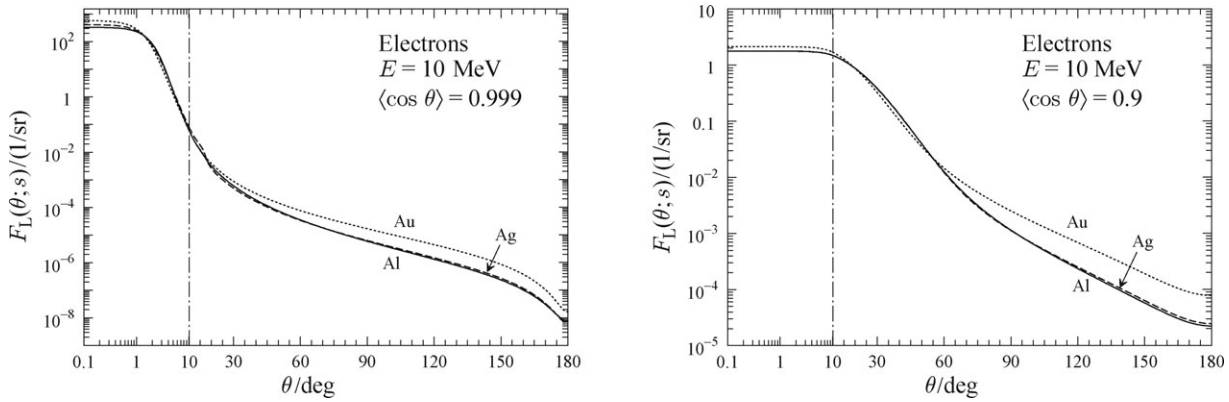

Figure 6.8 Multiple-scattering angular distributions of 10 MeV electrons in aluminum (solid line), silver (dashed line), and gold (dotted line) after traveling path lengths such that the average angular deflection $\langle\cos\theta\rangle$ equals the indicated values.

obtained from the partial-wave DCS and from the Wentzel–Molière model may differ appreciably.

As shown above [Eqs. (6.13) and (6.31)], the average angular deflection $\langle\cos\theta\rangle_L$ along the path length s is determined by the first transport coefficient $\mathcal{G}_1(s)$. In the multiple scattering regime, *i.e.*, when the average number of elastic collisions is of the order of 20 or larger, the 'width' of the angular distribution (and its height at small angles) is basically determined by the value of $\mathcal{G}_1(s)$. When the average angular deflection is small, the large-angle tail of the angular distribution is caused by electrons that have undergone a *single* large-angle deflection (because multiple large-angle interactions occur with much smaller probability) and, therefore, the angular distribution at large angles is essentially proportional to the single-scattering DCS. In practice, multiple-scattering distributions of electrons or positrons with different initial energies that travel different lengths in different materials but have the same average deflection $\langle\cos\theta\rangle_L$, have similar shapes. This situation is illustrated in Fig. 6.8, which displays angular distributions that were calculated with the program LEWIS for 10 MeV electrons in aluminum, silver and gold and path lengths s yielding the same average deflections.